14th International Conference on Applications of Statistics and Probability in Civil Engineering, ICASP14
Dublin, Ireland, July 9-13, 2023

Digital twin and SHM informed risk based inspection planning for offshore wind turbine structures

Thomas Bull
Ph.D. Candidate, Dept. of the Built Environment, Aalborg University & LICengineering, Esbjerg, Denmark

Daniel V. Muff
Engineer, LICengineering, Esbjerg, Denmark

Paul-Remo Wagner
Engineer, Matrisk, Zürich, Switzerland

Matthias Schubert
Engineer, Matrisk, Zürich, Switzerland

Hans Jørgen Riber
Engineer, LICengineering, Esbjerg, Denmark

Wei-Heng Zhang
Post doc., Dept. of the Built Environment, Aalborg University, Aalborg, Denmark

Michael H. Faber
Professor, Dept. of the Built Environment, Aalborg University, Aalborg, Denmark

ABSTRACT: Structural integrity management of wind turbine structures is typically based on equi-temporal inspection plans that do not account for the information that is or can be collected during their operation. This concerns the outcome of future inspections but also and very importantly the outcome of Structural Health Monitoring (SHM). Such information can be used within the framework of risk-based inspection (RBI) planning of structures to provide an information consistent basis for integrity management. In the present contribution we investigate how the concept of digital twins (DT) in conjunction with modern techniques of big data analysis may support this. The approach is demonstrated by a numerical example considering integrity management of a fatigue-sensitive detail of a 5MW reference offshore wind turbine support structure. The example results demonstrate the potential benefits of RBI planning and the value of taking into account the information from continuously collected SHM data.

1. INTRODUCTION

Fatigue-induced cracks in welded details of offshore wind turbines (OWTs) develop due to time variant operational and environmental loads acting on the structures throughout their service lives. Structural integrity management (SIM) procedures are extremely useful to ensure that the resulting fatigue crack growth is kept within acceptable safety and reliability limits. A typical SIM procedure for OWTs is to inspect potentially critical details at equi-distant times; however without quantifying the value added through the possibility to implement

risk reducing measures on the basis of future inspection outcomes. This approach which is common under most certification regimes can be improved substantially by utilizing experience from the oil and gas industry, where so-called risk-based inspection (RBI) procedures for SIM have successfully been implemented for most of the fixed steel oil and gas production facilities in the Danish part of the North-Sea, more than 100 fixed steel structures in the Mexican part of the Gulf of Mexico, and for several FPSO and FSO facilities (Faber et al., 2005; Goyet et al., 2004).

RBI procedures have evolved from their first industrial applications (Kirkemo, 1990; Sørensen et al., 1991) to more generic RBI approaches (Straub, 2004) to facilitate use by engineers without expertise in probabilistic modelling and fatigue crack growth. Among the various uncertainties that affect the RBI inspection plans, the uncertainties associated with the fatigue stresses acting on the critical locations of the welded details (the hot spots) play a key role. In presently applied RBI the stresses are modelled probabilistically, based entirely on design information regarding service life structural responses which in turn are derived from the nominal structural design. However, when the structures have been constructed and are in operation these probabilistic models may be updated through interpretation of observations from structural health monitoring (SHM). The potential of SHM as a means for SIM and the value of information (VoI) has been demonstrated on a broad range of structural systems, including wind turbine structures (Faber, 2017; Weijtjens et al., 2016; Maes et al., 2016; Nabuco et al., 2019).

Based on collected SHM information from structures in operation, it is also possible to gain an improved understanding of structural system characteristics and to update structural analysis models, e.g., finite element (FE) or RBI models, applied in the support of SIM. A calibrated, i.e., tuned to fit observations, FE model is often referred to as a digital twin (DT) of the physical system (Hofmeister et al. (2019)). The present paper investigates how a DT of the OWT can be constructed and, based on the information obtained from SHM, be updated such as to model structural responses that are probabilistically consistent with the SHM information. The DT is then used to model the probabilistic characteristics of the fatigue stresses in a hot spot and this model is in turn utilized as basis for developing an RBI plan. Finally the RBI plan is compared to a traditional RBI plan, based on design-phase stress estimates. The results are produced in a resilience-informed integrity management study on a monopile foundation of a 5MW generic OWT.

This paper is organized as follows: In Section 2, the DT-informed RBI planning framework is presented, Section 3 describes the numerical wind turbine setup and Section 4 presents the numerical example results. The paper is closed in Section 5 with the conclusions and an outlook to further developments of the proposed approach.

2. Digital twin-informed risk-based inspection planning

An illustration of the DT-informed framework, and how it compares to conventional RBI procedures based on conservative design model assumptions, is provided in Fig. 1. The prior model, already serving as basis for the design model assumptions in RBI schemes, is adapted to create a model database of realizations describing the possible OWT system characteristics. The model database is compared to the system characteristics estimated from the SHM measurements, hence identifying the models best describing what is observed. In the present paper, the DT corresponds to the model best describing observations and is used for the virtual sensing to achieve the stresses at hot spot locations. The full details of the SHM, DT and virtual sensing procedures for stress estimations are described in Section 2.1. The fatigue stress spectrum is finally utilized to develop an RBI plan as described in Section 2.2.

2.1. Digital twin-informed stress estimation

The SHM system collects n_k observations, where each observation $\mathcal{O}_k = \left\{\hat{U}_{10,k}, \ddot{\boldsymbol{u}}_k(t)\right\}$ comprises the 10-minute mean wind speed $\hat{U}_{10,k} \in \mathbb{R}$ and the 10-minute time series of acceleration measurements in n_m degrees of freedom (DOFs) $\ddot{\boldsymbol{u}}_k(t) \in \mathbb{R}^{n_m}$.

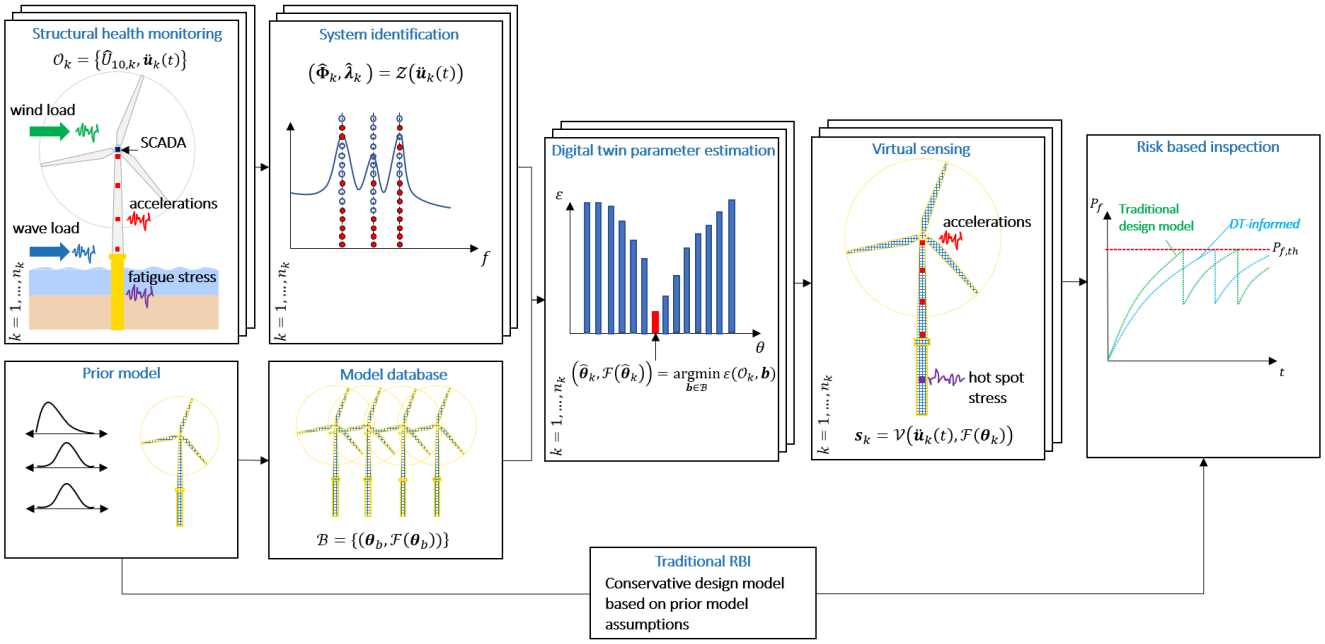

Figure 1: DT-informed and traditional RBI framework comparison.

These observations are then mapped to modal properties using a system identification procedure $\mathcal{Z}$ (see Section 2.1.1).

With a DT $\mathcal{F}(\hat{\boldsymbol{\theta}}_k)$ of the OWT, where $\mathcal{F}$ is an FE model and $\hat{\boldsymbol{\theta}}_k$ are the parameters that best explain the observations (see Section 2.1.2), the framework produces stress spectra $\boldsymbol{s}_k$ for each $k = 1, \ldots, n_k$:

$$\boldsymbol{s}_k = \mathcal{V}\left(\ddot{\boldsymbol{u}}_k(t), \mathcal{F}\left(\hat{\boldsymbol{\theta}}_k\right)\right) \tag{1}$$

where, $\mathcal{V}$ maps the accelerations $\ddot{\boldsymbol{u}}_k(t)$ and the DT $\mathcal{F}(\hat{\boldsymbol{\theta}}_k)$ to a stress spectrum using virtual sensing (see Section 2.1.3). These n_k spectra may then be combined to a combined spectrum $\boldsymbol{s}$ representing the stresses of the OWT during the observation period.

The three pillars of the stress-estimation approach (system identification, DT parameter estimation, and virtual sensing) are elaborated in the following.

2.1.1. System identification

System identification refers to the task of extracting system-related information, such as modal properties in the context of vibrating systems, based on an observed system response and, if possible, the excitation. In settings where ambient excitation sources govern the response, as is the case for OWT structures, only the response of the system is directly observable. In this case, assumptions regarding the nature of the excitation are imposed. Extraction of modal information from vibrating structures based solely on observed structural response is called operational modal analysis (OMA).

In the context of this paper, an automated operational modal analysis (AOMA) scheme is adopted:

$$(\hat{\boldsymbol{\Phi}}_k, \hat{\boldsymbol{\lambda}}_k) = \mathcal{Z}(\ddot{\boldsymbol{u}}_k(t)) \tag{2}$$

yielding n_j mode shapes $\hat{\boldsymbol{\phi}}_{k,j} \in \mathbb{C}^{n_m}$ and eigenvalues $\hat{\lambda}_{k,j} \in \mathbb{C}$ stored in $\hat{\boldsymbol{\Phi}}_k \in \mathbb{C}^{n_m \times n_j}$ and $\hat{\boldsymbol{\lambda}}_k \in \mathbb{C}^{n_j}$, respectively. Here, system identification is achieved through a data-driven subspace-based system identification (SSID) algorithm as described by van Overschee and Moor (1996). Subsequently, the identified poles (eigenvalues of estimated state matrices) are classified as either physical (kept) or spurious (discarded) based on an automated multi-stage clustering approach inspired by Reynders et al. (2012); Neu et al. (2017).

While the SSID algorithm provides numerical robustness, it also imposes the following assumptions: **(1)** the system behaves linearly and is time-invariant (LTI) and **(2)** the excitation resembles white noise.

Assumption **(1)** is violated when considering the operational changes (such as yaw and pitch) induced by changes in environmental conditions. However, for short time intervals (e.g., ten minutes) it is reasonable to assume that the processes describing the environmental conditions are stationary leading to approximately LTI system behavior.

Assumption **(2)** is violated by the wind and wave processes exciting the system (as well as rotor dynamics when the turbine is producing electricity). Consequently, modes not related to the structural modes of the wind turbine structure can be identified by the algorithm. However, as the dominating frequencies associated with wind, waves, and rotor dynamics are well known, from SCADA (supervisory control and data acquisition) and metocean data, these modes are readily identified and can be discarded if desired.

2.1.2. Digital twin parameter estimation

In practice, a DT is modelled to represent important aspects of the physical asset. In the context of stress estimation, the most important aspect is an accurate description of the structural response. To this end, the DT is formulated such that features that are known with high certainty, like the structural geometry, are fixed while more uncertain features that are also important for the structural response, such as soil conditions, are updated based on continuous monitoring. This ensures efficiency while retaining an accurate model for the purpose.

In this paper, parameter estimation is achieved by first populating a database $\mathcal{B} = \{(\boldsymbol{\theta}_b, \mathcal{F}(\boldsymbol{\theta}_b)) | b = 1,\dots,n_{\mathcal{B}}\}$ with numerical representations of the OWT for different sets of parameter realizations. Efficient population of the database can be achieved through well-known space filling design schemes. The parameters $\hat{\boldsymbol{\theta}}_k$ and corresponding FE model that best explain the observation $\mathcal{O}_k$ are then estimated by

$$(\hat{\boldsymbol{\theta}}_k, \mathcal{F}(\hat{\boldsymbol{\theta}}_k)) = \underset{\boldsymbol{b}\in\mathcal{B}}{\arg\min}\, \varepsilon(\mathcal{O}_k, \boldsymbol{b}) \tag{3}$$

where $\boldsymbol{b} = (\boldsymbol{\theta}_b, \mathcal{F}(\boldsymbol{\theta}_b))$ are the elements of the database and ε represents an appropriate distance metric. The approach for computing this metric is outlined in the following two steps. As we estimate optimal parameters based on a single set of observations, the subscript k is omitted for brevity.

Step 1 For each model $\mathcal{F}(\boldsymbol{\theta}_b)$ in $\mathcal{B}$, a modal subset $(\boldsymbol{\Phi}_b, \boldsymbol{\lambda}_b)$ comprising $n_i = 6$ modes $\boldsymbol{\phi}_{b,i} \in \mathbb{C}^{n_m}$ and $\lambda_{b,i} \in \mathbb{C}$, corresponding to the first three fore-aft (FA) and side-side (SS) modes, is considered. The contribution of each mode to the observed response $\ddot{\boldsymbol{u}}(t)$ is assessed through integration of the power spectral density. Weights $w_i^{(b)}$ are subsequently assigned to each mode based on their modal contribution.

Step 2 Following this, the n_j observed modal property-pairs $(\hat{\boldsymbol{\phi}}_j, \hat{\lambda}_j)$ from Eq. (2), as well as the 10-minute mean wind speed $\hat{U}_{10}$ are compared to the models in the database.

To this end, each mode i associated with the b-th database model is compared to a measured mode j using the following metric:

$$\delta_{i,j}^{(b)} = \delta_{\lambda,i,j}^{(b)} + \delta_{U_{10}}^{(b)}/10 + 1 - MAC_{i,j}^{(b)} \tag{4}$$

The terms in the metric correspond to relative distances between eigenvalues $\delta_{\lambda,i,j}$, 10-minute mean wind speeds $\delta_{U_{10}}$, and, finally, the modal assurance criterion (MAC) between mode shapes:

$$\delta_{\lambda,i,j}^{(b)} = \frac{\left|\lambda_{b,i} - \hat{\lambda}_j\right|}{\max\left\{\left|\lambda_{b,i}\right|, \left|\hat{\lambda}_j\right|\right\}} \tag{5}$$

$$\delta_{U_{10}}^{(b)} = \frac{\left|U_{10,b} - \hat{U}_{10}\right|}{\max\left\{U_{10,b}, \hat{U}_{10}\right\}} \tag{6}$$

$$MAC_{i,j}^{(b)} = \frac{\left|\boldsymbol{\phi}_{b,i}^H \hat{\boldsymbol{\phi}}_j\right|^2}{\boldsymbol{\phi}_{b,i}^H \boldsymbol{\phi}_{b,i} \hat{\boldsymbol{\phi}}_j^H \hat{\boldsymbol{\phi}}_j} \tag{7}$$

where $(\cdot)^H$ denotes the Hermitian transpose.

Mode i is compared to all n_j measured modes through Eq. (4) and the smallest distance from mode i to the observations is computed as

$$\delta_i^{(b)} = \min\left\{\delta_{i,j}^{(b)} | j = 1,\dots,n_j\right\} \tag{8}$$

Finally, the distance metric, including all six modes, is computed as

$$\varepsilon(\mathcal{O}_k, \boldsymbol{b}) = \sum_{i=1}^{6} \delta_i^{(b)} w_i^{(b)} \tag{9}$$

where $w_i^{(b)}$ are the weights computed in **Step 1**.

2.1.3. Virtual sensing

It is typically not feasible to instrument, and thereby directly monitor, all details of a physical system. Therefore, virtual sensing schemes are often adopted to estimate non-measured quantities based on a limited set of observations.

In the context of this paper, it is of interest to estimate stress spectra $\boldsymbol{s}_k = (\Delta\boldsymbol{\sigma}_k, \boldsymbol{N}_k)$ in the support structure using accelerations measured in the tower. The k-th spectrum comprises n_s stress ranges $\Delta\boldsymbol{\sigma}_k \in \mathbb{R}_+^{n_s}$ and associated numbers of cycles $\boldsymbol{N}_k \in \mathbb{R}_+^{n_s}$.

The modal expansion virtual sensing scheme is employed to estimate displacement response in the support structure by decomposition and subsequent extrapolation of the response using mode shapes. Using n_p modes for expansion and denoting the mode shape matrices from $\mathcal{F}\left(\hat{\boldsymbol{\theta}}_k\right)$ by $\boldsymbol{\Phi}_e \in \mathbb{R}^{n_e \times n_p}$ and $\boldsymbol{\Phi}_m \in \mathbb{R}^{n_m \times n_p}$, the estimated displacement response $\hat{\boldsymbol{u}}_k(t) \in \mathbb{R}^{n_e}$ in n_e DOFs is given by

$$\hat{\boldsymbol{u}}_k(t) = \boldsymbol{\Phi}_e \boldsymbol{\Phi}_m^{\dagger} \boldsymbol{u}_k(t) \tag{10}$$

where $(\cdot)^{\dagger}$ denotes a pseudo-inverse. Note that measured accelerations are converted to displacements $\boldsymbol{u}_k(t) \in \mathbb{R}^{n_m}$ through integration

$$\boldsymbol{u}_k(t) = \mathfrak{F}^{-1}\left(\frac{1}{-\omega^2}\mathfrak{F}\left(\ddot{\boldsymbol{u}}_k(t)\right)\right) \tag{11}$$

where ω, $\mathfrak{F}$ and $\mathfrak{F}^{-1}$ denote the angular frequency, the Fourier transform and its inverse, respectively.

The estimated displacements are subsequently converted to stress estimates using stiffness properties of the DT $\mathcal{F}(\hat{\boldsymbol{\theta}}_k)$.

It is evident that the LTI assumption is also implied when using modal expansion. As was argued in Section 2.1.1, violation of this assumption in the present application is limited because we consider short time intervals, where processes governing the non-linear and time variant behavior can be considered stationary.

2.2. Risk-based inspection

Risk-based inspection is a special application of Bayesian decision theory (Raiffa and Schlaifer, 1961) to determine the optimal strategy to inspect deteriorating structures (Straub and Faber, 2005). The RBI plans considered in this paper may also be called adaptive, because the RBI plan is updated during the lifetime of the structure by considering measurements of the structural performance (Bismut and Straub, 2021; Zhang et al., 2022).

RBI methods combine reliability assessment with probabilistic updating to establish a time-history of the reliability of hot spots, i.e., specific locations in the structure that are expected to have a high probability of failure. To this end, they rely on crack growth models to predict the crack evolution and detectable crack size models (probability of detection, PoD) to incorporate information obtained by inspection campaigns.

2.2.1. Crack-growth model

Steel structures can fail due to cyclic loading below their non-cyclic material strength. This failure mode is generally known as fatigue failure. There exist a variety of crack growth models (Richard and Sander, 2016; Rege and Lemu, 2017), but for this study the normalized crack growth model (NCGM) by Tychsen and Smedemark (2017) is used. It is a stochastic model that was fit to a large database of crack developments and was purpose-built for applications in inspection planning.

Given a stress spectrum and corresponding number of occurrences collected in a stress spectrum $\boldsymbol{s}$ the damage D of a hot spot is computed using a suitable S-N curve (e.g., from DNV-RP-C203 (2021)):

$$D(\boldsymbol{s}, \boldsymbol{x}_s) \tag{12}$$

where $\boldsymbol{x}_s$ is an uncertain parameter random vector specifying the S-N curve and its uncertainties. Given the damage, the NCGM can be used to com-

pute the crack length with

$$a(D,\alpha) = d_{\text{crit}} 10^{\frac{\log_{10}\left(\frac{D-\frac{\iota}{\alpha}}{1-\frac{\iota}{\alpha}}\right)}{\alpha(1+sD)f_{\text{plate}}}} \tag{13}$$

where d_{crit} is the critical crack depth at which failure occurs, f_{plate} is the plate-thickness factor that depends on the thickness of the hot spot plate, ι and s are fitting parameters. The stochasticity of the NCGM is induced by the uncertain α random variable that was fitted to observations in Tychsen and Smedemark (2017). Consequently, the model returns a random variable a for a given damage D.

2.2.2. Detectable crack size model

The quality of an inspection technique can be characterized through its PoD function. For a given crack length a, it returns the probability of detecting that crack with said inspection technique. The PoD used in this study is given by (Faber and Sørensen, 2002)

$$\text{PoD}(a) = 1 - \frac{1}{1+\left(\frac{a}{x_0}\right)^b} \tag{14}$$

where x_0 and b are parameters of the inspection method. This function can be inverted to obtain a probabilistic model of the detectable crack size with $c(u) = \text{PoD}^{-1}(u)$, where u is a standard uniformly distributed random variable.

2.2.3. Probability of failure

For a single hot spot and time t, we distinguish two types of events: failure F_t and inspection I_t. We further introduce the set of inspection times $\mathcal{T} = \{\tau_1, \ldots, \tau_{n.}\}$, that are prescribed or iteratively determined, and the set of inspections up until t as $\mathcal{I}_t = \{I_\tau | \tau \in \mathcal{T}, \tau \leq t\}$. The hot spot probability of failure at a certain time t given inspections until t may then be written as (after Straub (2011)):

$$\Pr\left(F_t | \mathcal{I}_t\right) = \frac{\Pr\left(F_t \cap \mathcal{I}_t\right)}{\Pr\left(\mathcal{I}_t\right)} \tag{15}$$

from which the annual failure probability can be derived as the time derivative.

These events are modeled here using a crack-growth model (see Section 2.2.1) and a detectable crack size model (see Section 2.2.2) that are parameterized with a random vector $\boldsymbol{X}\colon \Omega \to \mathcal{D}_{\boldsymbol{X}}$, where Ω denotes the probability sample space, with realizations $\boldsymbol{x} = (\boldsymbol{x}_s, \alpha, u)$, and joint probability distribution $f_{\boldsymbol{X}}(\boldsymbol{x})$. This random vector encodes the state of uncertainty related to the system.

The probabilities in Eq. (15) can be explicitly written as $\Pr(E) = \int_{\boldsymbol{x}\in\mathcal{D}_E} f_{\boldsymbol{X}}(\boldsymbol{x})\,\mathrm{d}\boldsymbol{x}$, by denoting the domain associated with an event E with $\mathcal{D}_E \subset \mathcal{D}_{\boldsymbol{X}}$. Estimating this probability integral is generally not possible in closed form. Instead, numerical methods of structural reliability may be used for maximum flexibility in terms of the event parametrization. Reviews of available methods in this field can be found in Rackwitz (2001); Jiang et al. (2017); Afshari et al. (2022).

With the S-N curve from Eq. (12) and a stress spectrum $\boldsymbol{s}_t$ at time t, the failure domain is

$$\mathcal{D}_{F_t} = \{D(\boldsymbol{s}_t, \boldsymbol{x}_s) > 1 | (\boldsymbol{x}_s, \alpha, u) \in \mathcal{D}_{\boldsymbol{X}}\} \tag{16}$$

For a given inspection result $r \in \{\text{detection}, \text{no detection}\}$, the damage D_t at time t combined with the crack growth model from Eq. (13), the inspection event domain for no detection is

$$\mathcal{D}_{I_t,\sim\text{detect}} = \{a(D_t,\alpha) < c(u) | (\boldsymbol{x}_s, \alpha, u) \in \mathcal{D}_{\boldsymbol{X}}\} \tag{17}$$

and analogously for the detection case.

3. NUMERICAL EXAMPLE SETUP

The case study is a comparison between traditional RBI based on design model stress simulations and DT-informed RBI based on SHM measurements. Both stress estimates are obtained from simulations using a generic 5MW reference wind turbine installed on a fixed bottom monopile foundation and exposed to a typical fatigue limit state (FLS) load case. Variation of the soil strength as well as operational variability (induced by changing wind) is considered in the measurement simulations; the wind and wave loading follow the design assumptions. The depth-dependent soil strength is scaled by a multiplier following a log-normal distribution with a mean of 1 and a coefficient of variation (COV) of 0.33, Jones et al. (2002), while

the design estimate uses a deterministic soil corresponding to the 5% quantile of the distribution (which is considered conservative).

The simulations are computed with the open-source software package OpenFAST (NREL, 2022), a simulation tool for dynamic responses of wind turbines. The wind turbine is the 5MW NREL wind turbine with a rotor radius of 63 m and a hub height of 90 m. The monopile has diameter of 6 m, wall thickness of 50 mm and a total height of 60 m with a 30 m soil penetration. The soil-structure interaction is modelled by linearized soil curves. The structural damping is modelled by a Rayleigh model assuming 1 % damping on the first and second bending modes. The wind turbine is assumed installed at a position in the Danish waters with a water depth of 20 m. The metocean and soil data are based on site specific data at a region in the Baltic Sea. The wind is simulated according to the DNV with the IEC normal turbulence model while waves are simulated using first-order theory and the JONSWAP spectrum.

Displacements and accelerations are assumed measured by bi-axial sensors at four different elevations on the turbine tower, see Fig. 2.

The DT database $\mathcal{B}$ is populated (utilizing Latin hypercube sampling) with 750 realizations of soil and wind speed parameters according to their probability distribution. Wind speed is used as a proxy for rotor speed and pitch based on the linearization feature of OpenFAST (Jonkman et al., 2018). The mapping from the database is based on the system identification of the observed accelerations according to Section 2.1, while the modal expansion is performed based on the displacements.

To construct the RBI plan, a constant annual reliability threshold approach is applied with an inspection threshold of 10^{-4}. The SN-curve D from DNV-RP-C203 (2021) is adopted with parameters $m_1 = 3$, $m_2 = 5$, $d_{\text{ref}} = 25\,\text{mm}$, and $k = 0.2$. The parameters $\boldsymbol{x}_s$ with components $\log\bar{a}_1$ and $\log\bar{a}_2$ are treated as uncertain and follow a Gaussian distribution with mean 11.764 and 15.606, respectively, and a COV of 3 %. The parameters of the NCGM are selected as $d_{\text{crit}} = 50\,\text{mm}$, $f_{\text{plate}} = 1.15$, $s = -0.565$, and $\iota = 0.1$. The parameters

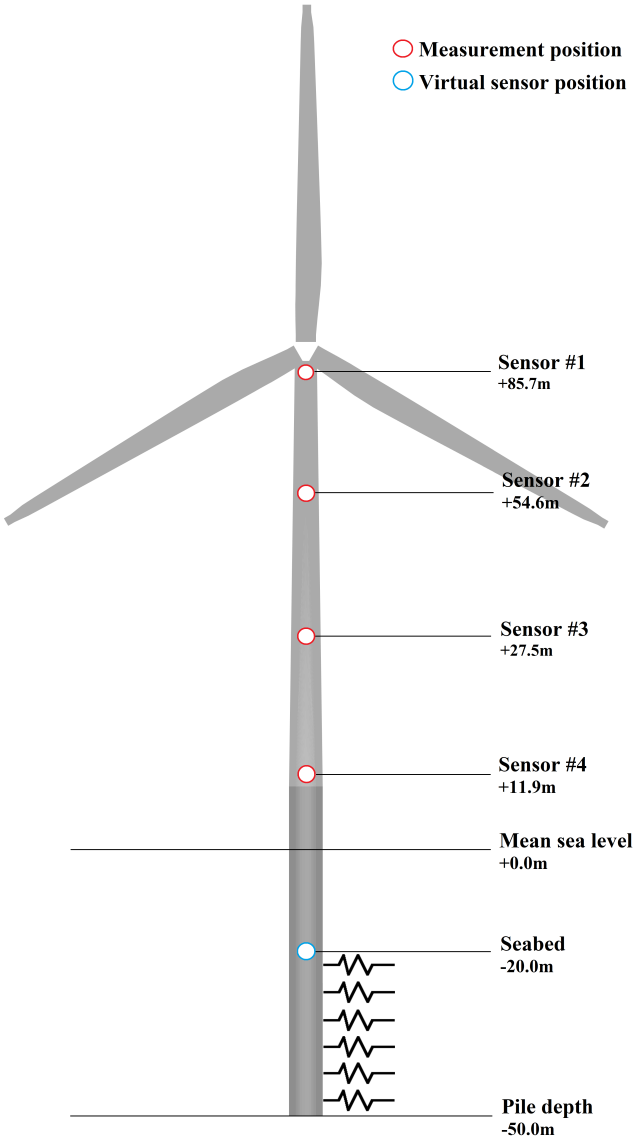

Figure 2: Wind turbine and sensor positions.

of the PoD curve are selected as $x_0 = 1.4$, $b = 2$. The stress-concentration factor is selected as uncertain following a Gaussian distribution with mean 1.07 (DNV-RP-C203, 2021) and standard deviation 0.05.

4. Numerical example results

The RBI results, as illustrated in Fig. 3, show an evident improvement in the inspection plans when using the DT-informed stress estimates over using design model estimates when comparing with the annual probability of failure for the fatigue sensitive detail.

The design stress estimate schedules the first in-

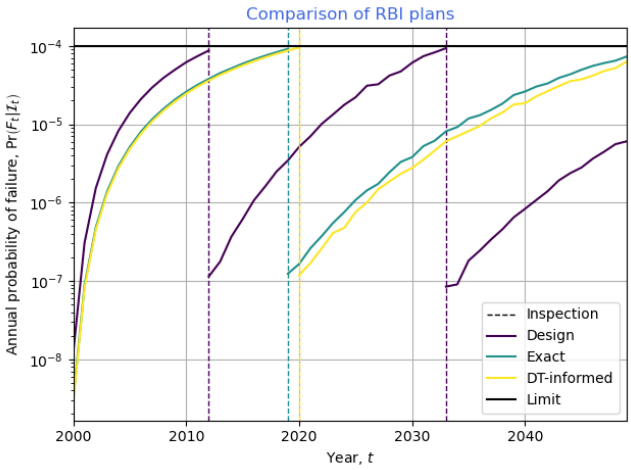

Figure 3: RBI plan with annual probability of failure as a function of time based on stress spectra from the DT-informed approach (yellow), the design model approach (purple), and the exact spectra (blue).

spection seven years earlier than otherwise prescribed by the plan derived from the exact stresses, revealing that the stress estimates are indeed conservative. As expected, the DT-informed stress estimate is better aligned with the actual stresses.

It should be noted that the same uncertainties have been applied in the RBI for all three inspection plans to allow for a direct comparison.

5. Conclusions

The value of installing a SHM measurement system and taking benefit of the information in a DT setup is highly dependent on the bias in the design model assumptions. However, the bias is hard to quantify without any information of the system performance after installation. In the present numerical example we demonstrate that the number of inspections for integrity management of wind turbine support structures can be significantly reduced, hence clearly illustrating the potential and value of introducing SHM measurement systems in combination with RBI models. The procedure can also prove beneficial in the opposite case, where the design assumptions are non-conservative, as the reliability of the structure is updated and an increased number of inspections would be performed according to the actual utilization level.

Furthermore, the SHM measurements allow for detection of any anomalies during operation of the wind turbine and can update the inspections of the structure due to changes in either load environment or the structure itself. The SHM-DT setup also allows for updating and propagation of uncertainties based on the observations using big data techniques and probabilistic methods, such as those presented in Glavind et al. (2022); this will be further investigated in a subsequent paper.

6. REFERENCES

Afshari, S. S., Enayatollahi, F., Xu, X., and Liang, X. (2022). "Machine learning-based methods in structural reliability analysis: A review." *Reliability Engineering & System Safety*, 219, 108223.

Bismut, E. and Straub, D. (2021). "Optimal adaptive inspection and maintenance planning for deteriorating structural systems." *Reliability Engineering & System Safety*, 215, 107891.

DNV-RP-C203 (2021). "Fatigue design of offshore steel structures." *Standard*, Det Norske Veritas.

Faber, M. H. (2017). "Risk informed structural systems integrity management: A decision analytical perspective." *Proceedings of the ASME 2017 36th International Conference on Ocean, Offshore and Arctic Engineering*, 9.

Faber, M. H. and Sørensen, J. D. (2002). "Reliability and risk based inspection planning for jacket structures.

Faber, M. H., Sørensen, J. D., Tychsen, J., and Straub, D. (2005). "Field implementation of RBI for jacket structures." *Journal of Offshore and Arctic Engineering*, 127(3), 220–226.

Glavind, S. T., Sepulveda, J. G., and Faber, M. H. (2022). "On a simple scheme for systems modeling and identification using big data techniques." *Reliability Engineering and System Safety*, 220.

Goyet, J., Rouhan, A., and Faber, M. H. (2004). "Industrial implementation of risk based inspection planning methods – Lessons learnt from experience: The case of FPSOs." *Proceedings of the 23rd International Conference on Offshore Mechanics and Arctic Engineering*, 2, 553–563.

Hofmeister, B., Bruns, M., and Rolfes, R. (2019). "Finite element model updating using deterministic optimisation: A global pattern search approach." *Engineering Structures*, 195, 373–381.

Jiang, Z., Hu, W., Dong, W., Gao, Z., and Ren, Z. (2017). "Structural reliability analysis of wind turbines: A review." *Energies*, 10(12), 2099.

Jones, A. L., Kramer, S. L., and Arduino, P. (2002). "Estimation of uncertainty in geotechnical properties for performance-based earthquake engineering." *Report*, University of Washington.

Jonkman, J. M., Wright, A. D., Hayman, G. J., and Robertson, A. N. (2018). "Full-system linearization for floating offshore wind turbines in openfast." *Proceedings of the ASME 2018 1st International Offshore Wind Technical Conference*.

Kirkemo, F. (1990). "Probabilistic strategy increases jacket in-service inspection efficiency." *Offshore*, 50(12), 46–47.

Maes, K., Iliopoulos, A., Weijtjens, W., Devriendt, C., and Lombaert, G. (2016). "Dynamic strain estimation for fatigue assessment of an offshore monopile wind turbine using filtering and modal expansion algorithms." *Mechanical Systems and Signal Processing*, 76-77, 592–611.

Nabuco, B., Faber, H. B. M. H., and Brincker, R. (2019). "A first step in quantifying the value of oma based fatigue stress estimation." *8th International Operational Modal Analysis Conference*, 645–652.

Neu, E., Janser, F., Khatibi, A. A., and Orifici, A. C. (2017). "Fully automated operational modal analysis using multi-stage clustering." *Mechanical Systems and Signal Processing*, 84(A), 308–323.

NREL (2022). "OpenFAST – Open-source wind turbine simulation tool." *v3.2.1*.

Rackwitz, R. (2001). "Reliability analysis – a review and some perspectives." *Structural Safety*, 23(4), 365–395.

Raiffa, H. and Schlaifer, R. (1961). *Applied statistical decision theory*. Harvard University, fifth edition.

Rege, K. and Lemu, H. G. (2017). "A review of fatigue crack propagation modelling techniques using FEM and XFEM." *IOP Conference Series: Materials Science and Engineering*, 276, 012027.

Reynders, E., Houbrechts, J., and Roeck, G. D. (2012). "Fully automated (operational) modal analysis." *Mechanical Systems and Signal Processing*, 29, 228–250.

Richard, H. A. and Sander, M. (2016). *Fatigue crack growth*. Springer International Publishing.

Straub, D. (2004). "Generic approaches to risk based inspection planning for steel structures." Ph.D. thesis, ETH Zurich,

Straub, D. (2011). "Reliability updating with equality information." *Probabilistic Engineering Mechanics*, 26(2), 254–258.

Straub, D. and Faber, M. H. (2005). "Risk based inspection planning for structural systems." *Structural Safety*, 27(4), 335–355.

Sørensen, J. D., Rackwitz, R., Faber, M. H., and Thoft-Christensen, P. (1991). "Modelling in optimal inspection and repair." *Proceedings of the 10th International Conference on Offshore Mechanics and Arctic Engineering*, 2, 281–288.

Tychsen, J. and Smedemark, J. (2017). "Development of normalized stochastic fatigue crack growth model." *Report No. TE17-128/JPT003, Rev. 0., 8th Dec. 2017*, Maersk Oil (dec).

van Overschee, P. and Moor, B. D. (1996). *Subspace Identification for Linear Systems*. Kluwer Academic Publishers, 57–94.

Weijtjens, W., Verbelen, T., Sitter, G. D., and Devriendt, C. (2016). "Foundation structural monitoring of an offshore wind turbine – A full-scale case study." *Structural Health Monitoring*, 15(4), 489–502.

Zhang, W.-H., Qin, J., Lu, D.-G., Liu, M., and Faber, M. H. (2022). "VoI analysis of temporally continuous SHM information in the context of adaptive risk-based inspection planning." *Structural Safety*, 99, 102258.